

CAAP Quarterly Report
January 25, 2024

Project Name: Selection and Development of Safer Polymer and Composite Pipeline Liners through Microstructural and Macroscopic Study of Materials and Designs

Contract Number: 693JK32250001CAAP

Prime University: Brown University

Prepared By: Ryan Poling-Skutvik, Edith Mathiowitz, and Vikas Srivastava

Ryan Poling-Skutvik, Ph.D.

Email: ryanps@uri.edu

Phone: 401-874-2627

Edith Mathiowitz, Ph.D.

Email: Edith_Mathiowitz@brown.edu

Phone: 401-863-1358

Vikas Srivastava, Ph.D.

Email: vikas_srivastava@brown.edu

Phone: 401-863-2863

Reporting Period: October 1, 2023 – December 31, 2023 (Q3)

Project Activities for Reporting Period:

All four types of polymers were acquired and polyethylene, epoxy, and polyamide and PVDF were partially analyzed through DSC, ATR, and X-ray diffraction. DSC results are for unprocessed raw polymer, ATR results are for melt cast samples with no processing, and XRD results are for both melt cast and processed samples. The thermal history can be seen in the first melt scan in the DSC for each polymer. The nature of the flat thin disks that result from melt casting made ATR the best analysis tool. These are compared to FTIR data from the literature which is more readily available so peak shapes and sizes may vary but band location should be the same across both methods.

We can see for the polyethylene that the spectrum closely matches both LDPE and HDPE which is unsurprising given their very similar composition. However, we can see a peak at approximately 1377 cm^{-1} that is present in Figure 1 and the literature data in Figure 3 that is not seen in HDPE scans in Figure 2. While alone not enough to make the determination usually, it corresponds to DSC thermal properties seen in Figure 4, with a significantly lower melting temperature than would be expected for an HDPE sample as seen in Figure 5. Using the enthalpy of a 100% crystalline sample a crystallinity of 17% was calculated [1], lower than the expected LDPE crystallinity of ~30%, and much lower than the expected 80% of HDPE.

Polyamide samples showed many of the expected peaks in the ATR scan and were verified by the literature, however based on the ATR it is difficult to determine if it is PA12, PA6 or other polyamides. The DSC provided more conclusive information showing a melt temperature of 177°C which corresponds to the expected melt temperature of PA12 at 180°C. PA6 has an expected melt temperature of 230°C and PA11 of 190°C. An expected glass transition for polyamide 12 at 50°C was not detected in scans done. A comparison of the experimental DSC seen in Figure 9 and the scan of different cast times Figure 10 we can see the effects of previous processing with a single peak being seen on the first heating but transitioning to a broader two-part peak at a lower casting temperature. This single peak is indicative of a gamma crystal structure being formed while the dual peak is indicative of alpha crystal forms. Based on this information the raw polymer we received was processed at a relatively high temperature and was cooled very slowly giving a peak similar to the casting at hot temperature seen in Figure 10. The cooling of the DSC occurs at 10°C/minute, likely faster than allowed at manufacturing, producing a subsequent heating profile more similar to the polymer cast at a lower temperature.

PVDF filament was received and analyzed through DSC and XRD. Literature indicates the melt temperature of PVDF to be 173°C [2]. The melt temperatures in the DSC scan in Figure 13 showed a melt peak at 167°C for the melt cast and 169°C and 165°C for subsequent scans at different heating rates. There was also the appearance of a dual peak at the melt for 30°C/min and 50°C/min which may indicate distinct crystalline phases. X-ray diffraction was conducted on both melt cast and heat pressed samples. In Figure 14 changes in the intensity at 19°, 20° and 23° could be seen, with processing at 170°C yielding the highest intensity for peaks at 19° and 20° and samples processed at 190°C showing nearly no diffraction at 23°. PVDF is a complex polymer with multiple polymorphisms and 3 common crystal phases meaning the changes in T_m and melt shape can be a result of changes in both crystallinity percentage or crystalline phase transitions [3].

Epoxies have the greatest potential for variation of our polymers and are also the only thermosetting polymer we are currently using. The ATR scans seen in Figures 16 and 17 show many key regions that are still present in epoxies from literature and our experimental data. DSC scans showed no thermal events such as melting or glass transition which to be expected with a thermoset polymer and indicates that the casting period of 6 hours is enough for the sample to fully solidify.

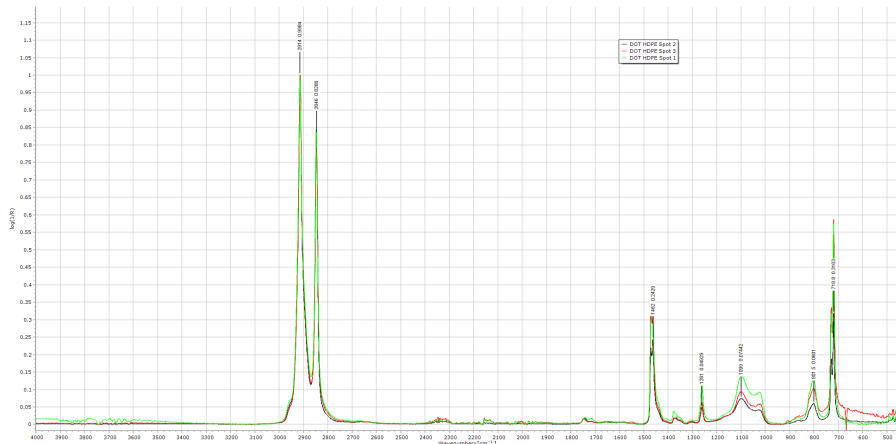
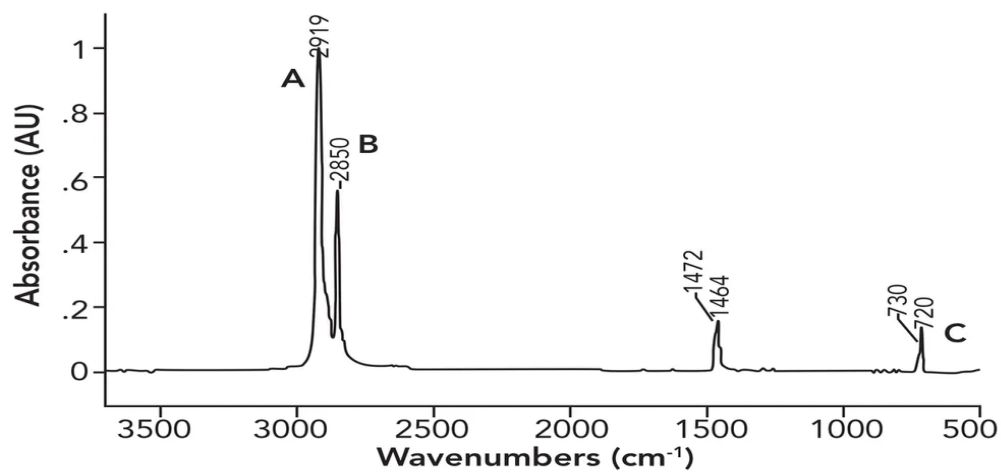
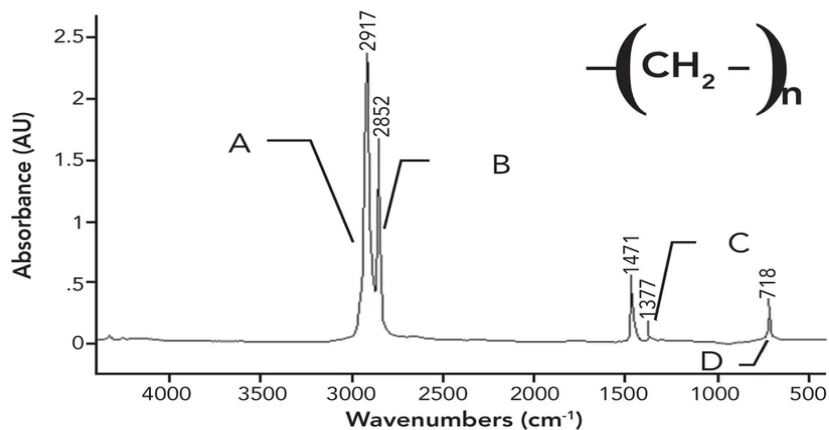


Figure 1. Received polyethylene ATR spectra (N=3).



A	2919	CH ₂ Asymmetric C-H stretch
B	2850	CH ₂ Symmetric C-H stretch
C	730, 720	Split CH ₂ rock

Figure 2. HDPE ATR spectra from literature [4].



A	2917	CH ₂ Asymmetric C-H stretch
B	2852	CH ₂ Symmetric C-H stretch
C	1377	CH ₃ Umbrella mode
D	718	CH ₂ Rock

Figure 3. LDPE ATR spectra from literature [4].

While LDPE and HDPE are very similar under ATR scans due to the similarity of the CH₂ bonds, small differences can be used to distinguish the two polymers. A peak at approximately 1377 cm⁻¹ that is present in Figure 1 and the literature data in Figure 3 that is not seen in HDPE scans in Figure 2 is a result of the CH₃ umbrella and more branching nature of LDPE presenting more of these groups than in an HDPE sample. The single peak present at ~1470 cm⁻¹ also points to LDPE where a split peak would indicate longer, more crystalline chains indicative of HDPE.

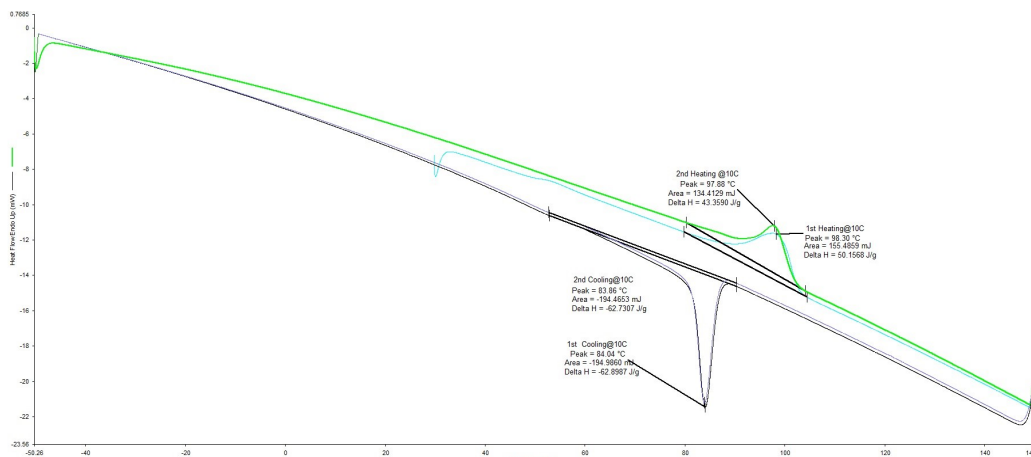


Figure 4. Received polyethylene DSC scan.

Table 1. DSC Results for received polyethylene.

Event	Order	Temperature (°C)	Enthalpy (J/g)
Melt Peak	First Heating	98.3	50.1
	Second Heating	97.8	43.3
Crystallization	First Cooling	84.0	-62.9
	Second Cooling	83.6	-62.7

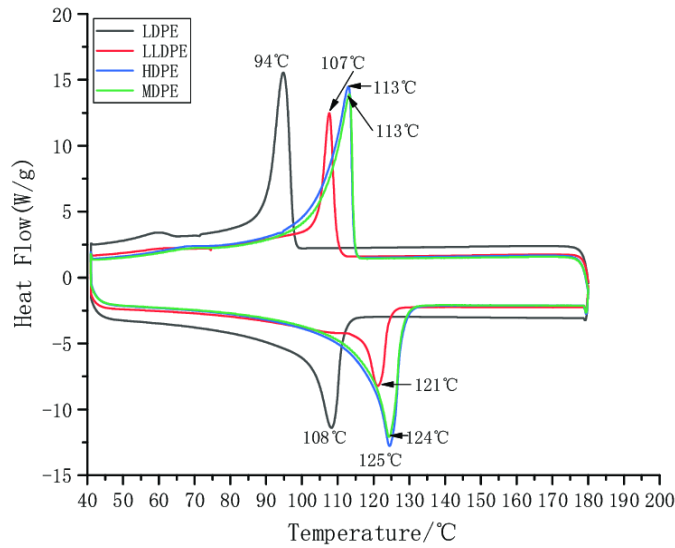


Figure 5. DSC curves found in literature for polyethylene [5].

DSC thermal properties seen in Figure 4 and summarized in Table 1, show a significantly lower melting temperature than would be expected for an HDPE sample as seen in Figure 5. Using the enthalpy of melt and recrystallization a crystallinity of 17% was calculated for the received sample. Expected crystallinities for LDPE is while for HDPE it is lower than the expected LDPE crystallinity of 20-40%%, and much lower than the expected 60-80% of HDPE [6].

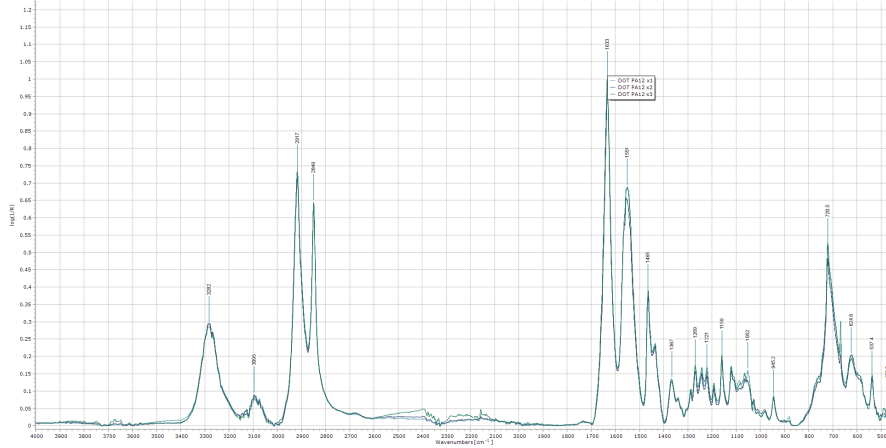


Figure 6. Experimental PA12 ATR Spectra (N=3).

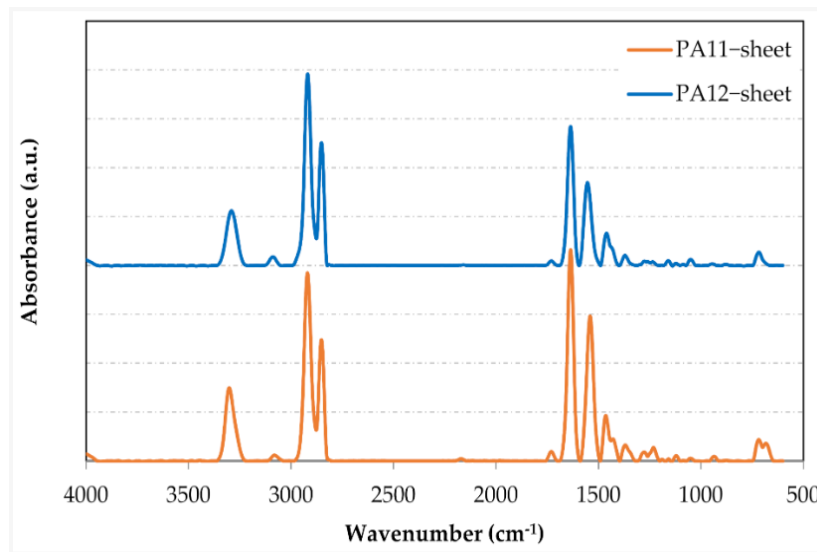


Figure 7. PA12 Spectra from literature [7].

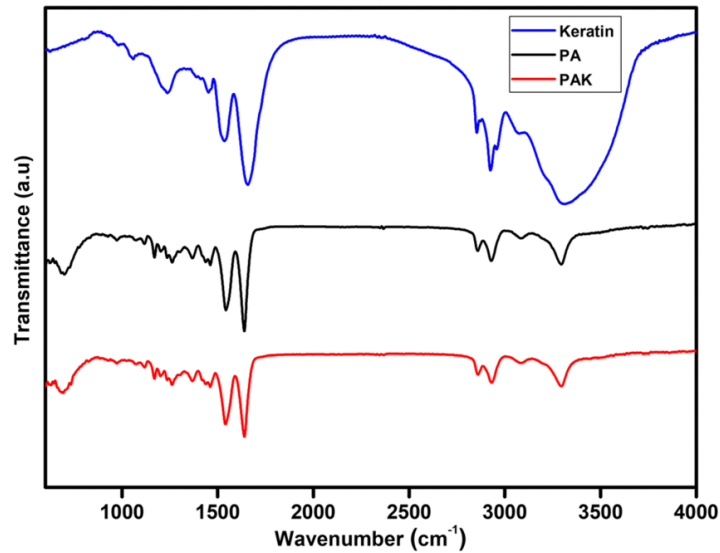


Figure 8. PA6 from literature [8].

The spectra bands for the received polyamide were observed at $\sim 1635\text{ cm}^{-1}$, $\sim 1540\text{ cm}^{-1}$, and $\sim 1275\text{ cm}^{-1}$ which correspond to amide I, II and III, respectively. Additional bands at 2850 cm^{-1} and 2920 cm^{-1} correspond to the vibrating C-H bond which is present in all polyamide samples. This allows for identification of the sample as a polyamide but limits further specification.

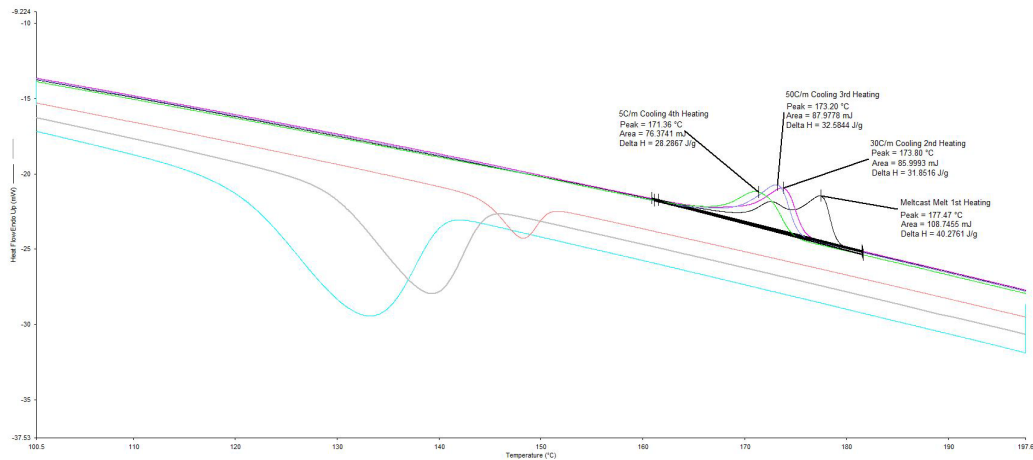


Figure 9. Received polyamide DSC at different heating rates.

The DSC shows a melting point of around 177C for the melt cast polyamide samples and a melting point of 173C for subsequent remelts of the sample. This corresponds to the accepted melting point of PA12 at 178-180C which is among the lowest of polyamides indicating it is not a copolymer blend.

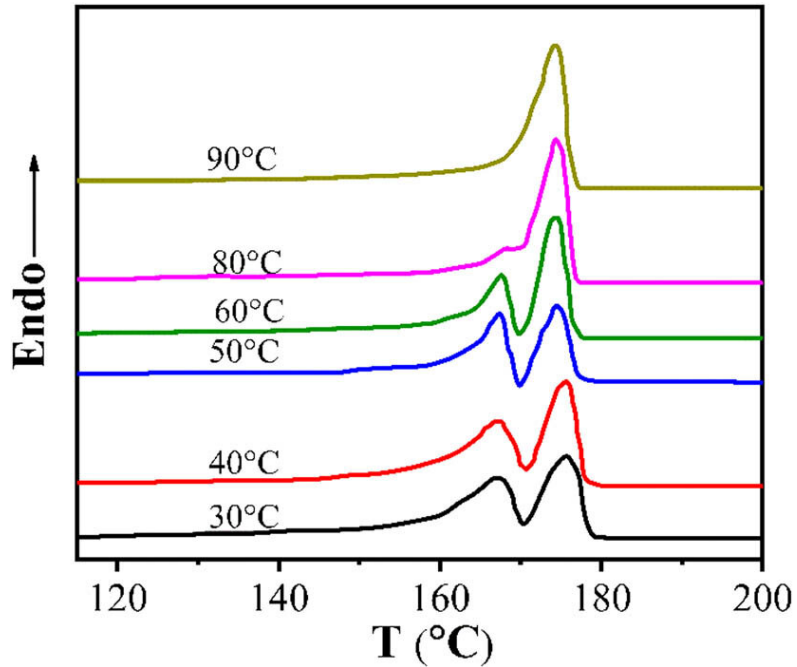


Figure 10. PA12 DSC at different cast temperatures [9].

Figure 10 show a DSC scan of PA12 which was melt cast and then kept at the indicated temperatures until it solidified. This results in different crystallization planes as the chain align. The data from both MJ and Zakhar indicate that the sample previously purchased that was assumed to be HDPE is in fact LDPE.

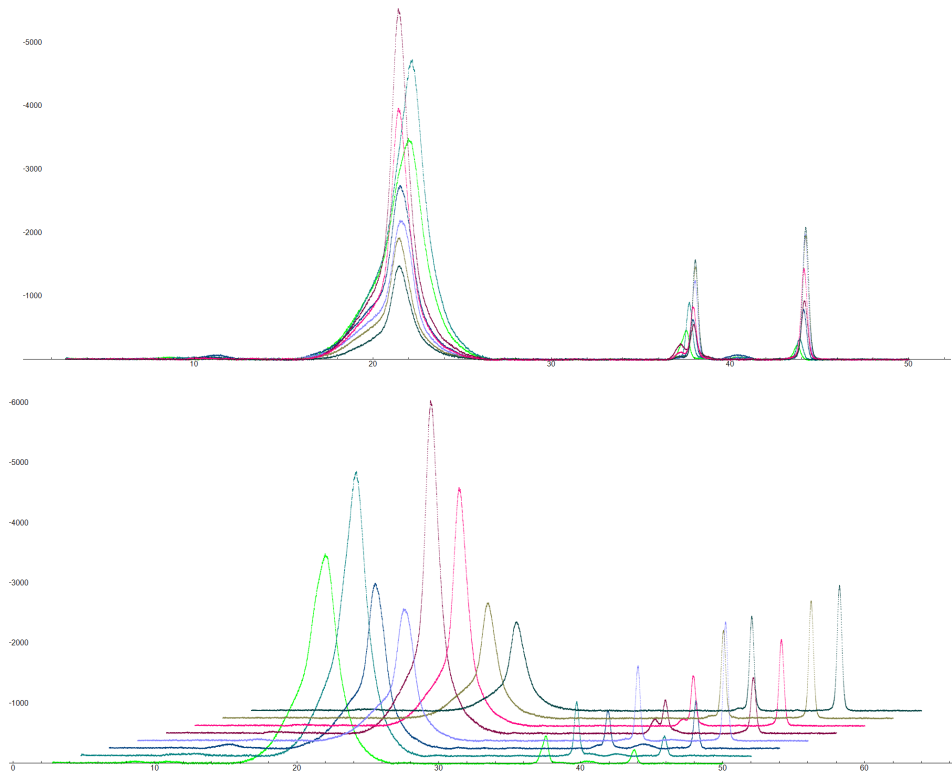


Figure 11. XRD spectra of PA12 heat pressed at 10000lbs at 165 (bottom left), 170, 175, 180, 185, 190, 195, and 200°C.

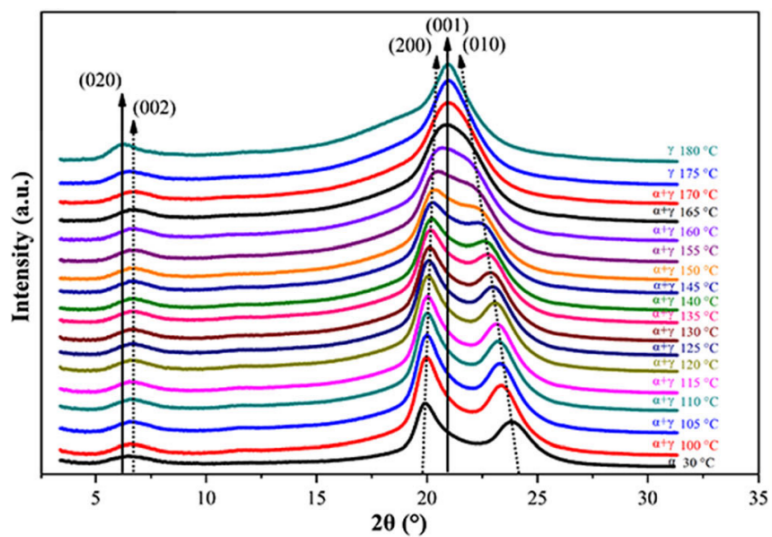


Figure 12. XRD spectra of PA12 cast at various temperatures solution casting XRD [9].

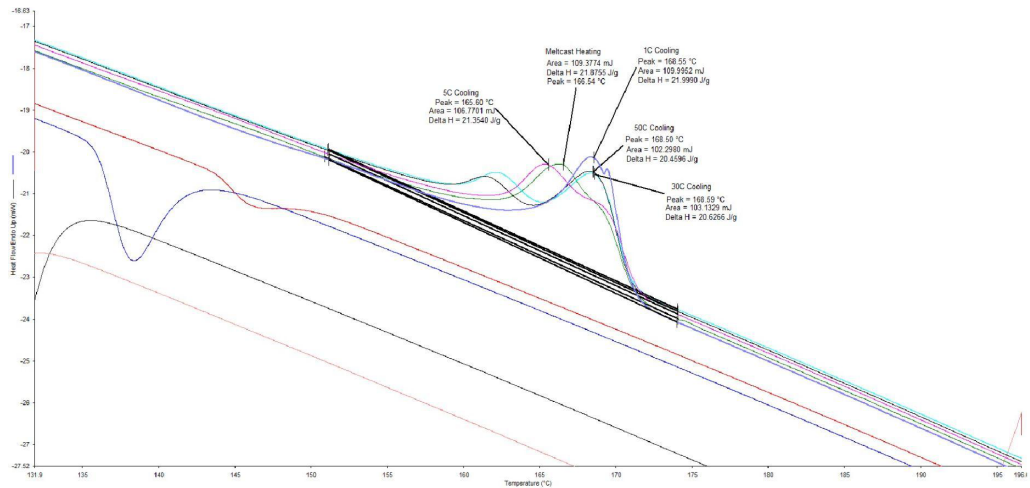


Figure 13. DSC of PVDF at different cooling rates.

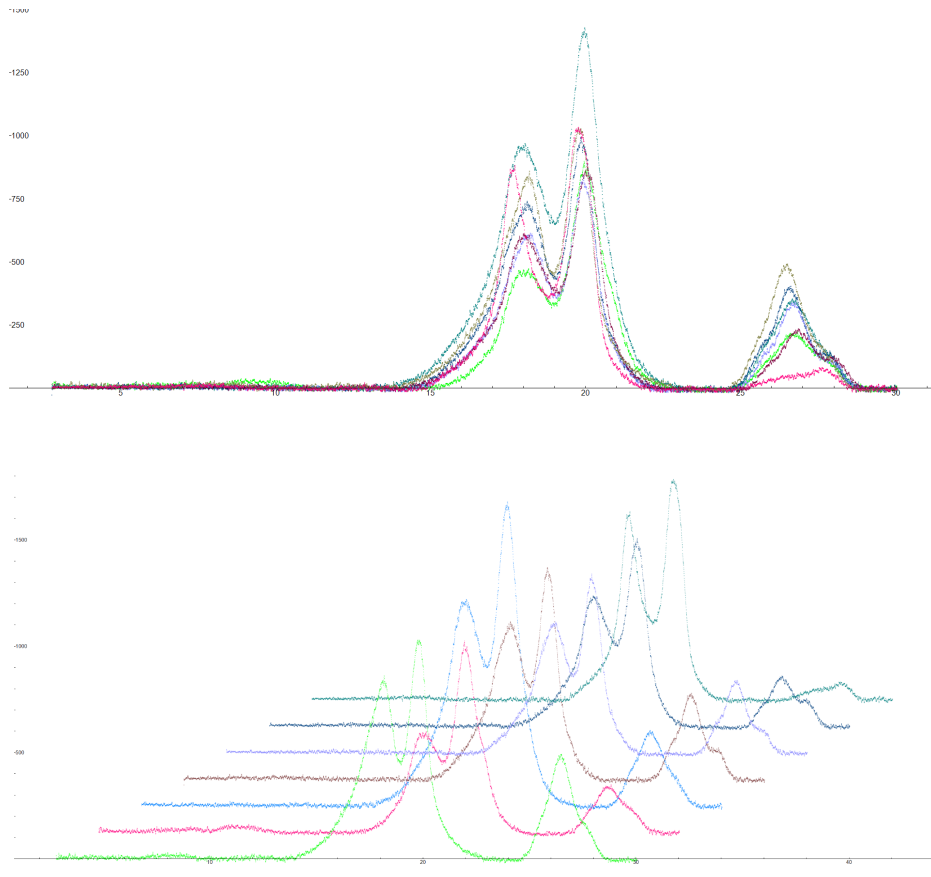


Figure 14. XRD spectra of PVDF melt cast (bottom left) and heat pressed at 10000lbs at 165, 170, 175, 180, 185, 190°C.

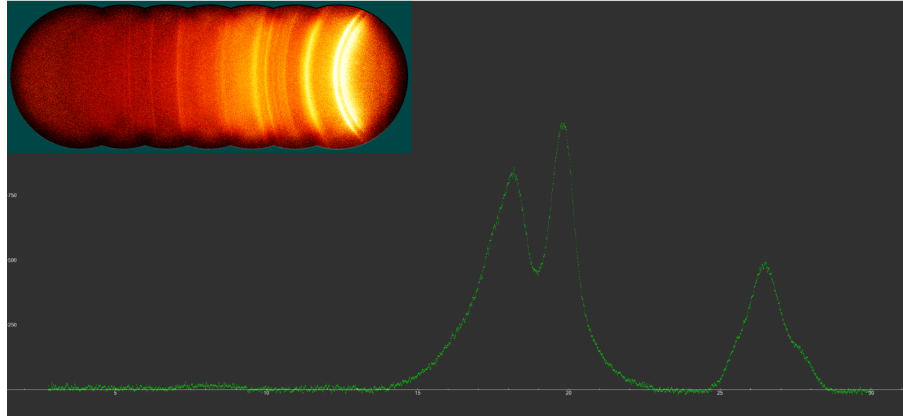


Figure 15. 2D spectra and X-ray spectra of melt cast PVDF.

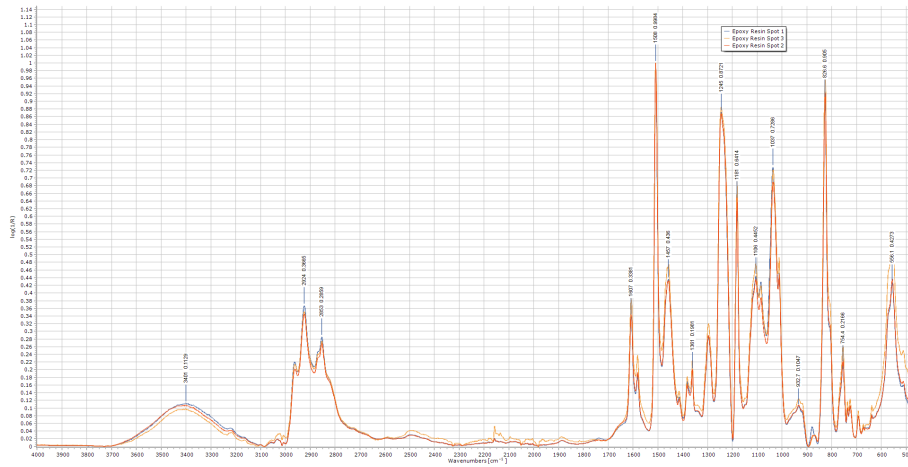


Figure 16. Experimental Epoxy FTIR.

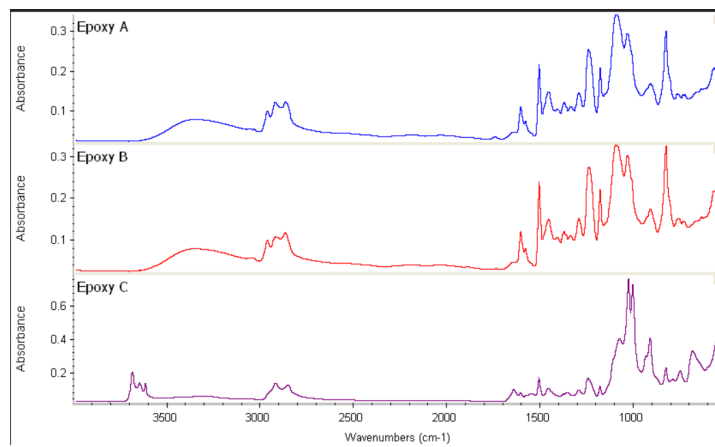


Figure 17. FTIR of several unknown epoxies from literature [10].

At present, the hydraulic press and molds are utilized to produce three distinct types of samples. The first type is the rectangular samples designed for Dynamic Mechanical Analysis (DMA) testing. The second type, referred to as type V samples, is intended for tensile testing. The third type consists of circular samples with varying diameters, tailored for conducting a range of rheological and mechanical tests.

Figure 18 depicts the DSC result for the acquired HDPE. It is obvious that the material exhibits a melting point at 135°C. By employing the enthalpy value of 100% crystalline HDPE, which is 293 J/g, the calculated crystallinity of the HDPE is approximately 63%. This crystallinity is near the reported values in the literature.

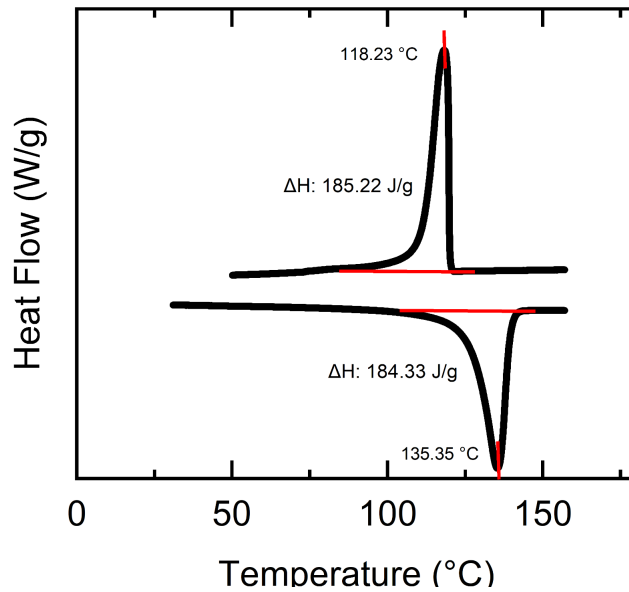


Figure 18. DSC diagram of the purchased HDPE.

Activation energy for HDPE was determined through Frequency Sweep tests conducted at temperatures ranging from 130 to 170°C. The Arrhenius model was employed for this analysis. Figure 19 presents the HDPE activation energy, showing a proximity to the literature value of 29.3 kJ/mol [11]. It is important to note that polymers do not possess a constant activation energy, as it is contingent upon various properties of the polymer grade.

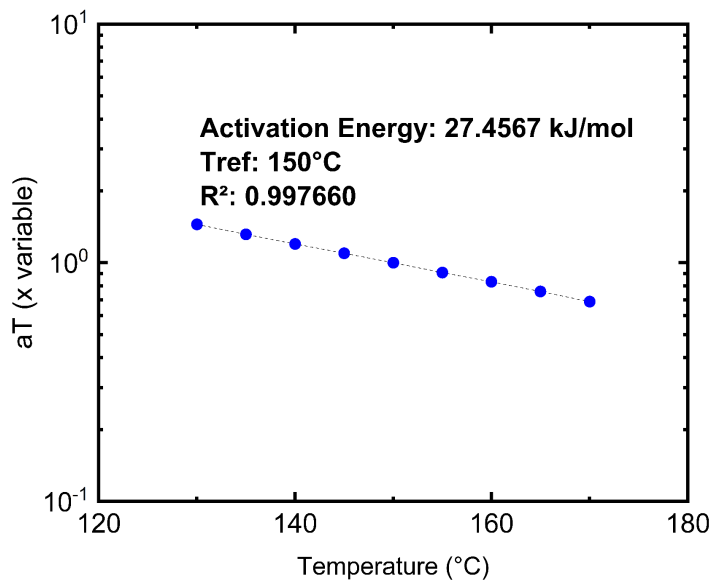


Figure 19. Activation energy of HDPE measured with the use of the Arrhenius model in the range of 170 to 130°C.

Furthermore, a series of creep tests were conducted. Creep is the time-dependent change in strain due to a constant applied stress. For an idealized creep strain curve as shown in Figure 20, the primary or transient state of creep is characterized by a rapidly decreasing creep rate. In secondary creep, the creep strain rate reaches a steady-state value and is followed by the tertiary creep, where a rapid increase in creep strain rate occurs until fracture or rupture of the material.

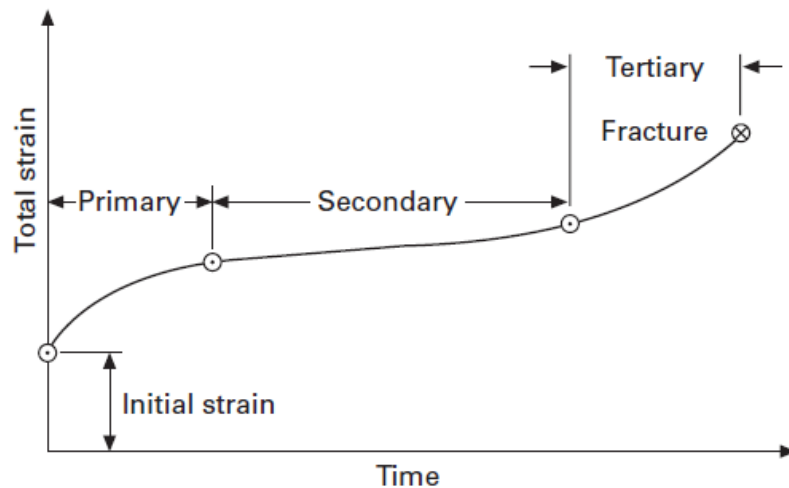


Figure 20. Typical creep strain response of a material with constant applied load [12].

Creep assumes a pivotal role in the design of plastic products, serving as an indicator of their load-bearing capacity. There are some challenges in structural designs because of the creep rupture and other time-dependent failures that affect the product lifespan. To ensure longevity and mitigate premature failures accompanied by excessive deformation, a critical step involves evaluating durability during the design phase. This can be done with the time-temperature superposition principle. By employing this method, it becomes feasible to anticipate the long-term creep behavior of polymers through measurements conducted at higher temperatures.

Figures 21 and 22 illustrate the application of this method on a prototype material. The compliance curves, obtained at various stress levels and the same temperature, can be superimposed onto a master curve which covers a wider time range at a reference stress.

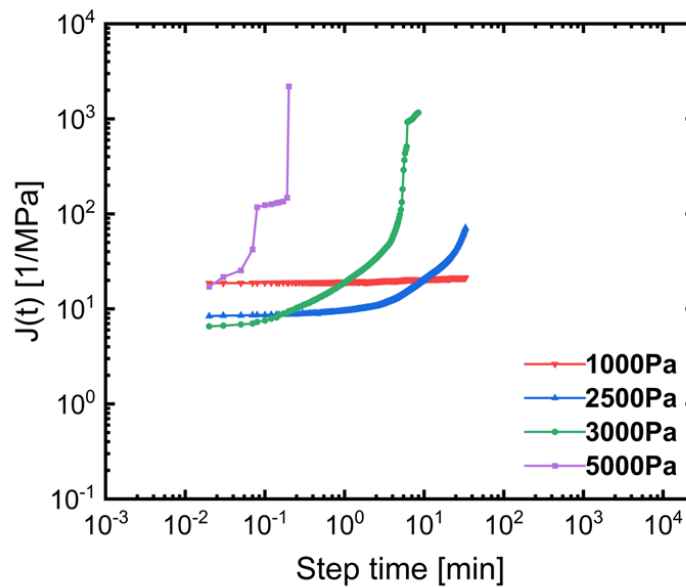


Figure 21. Compliance ($J(t)$) of the prototype sample at different stress levels at 110°C.

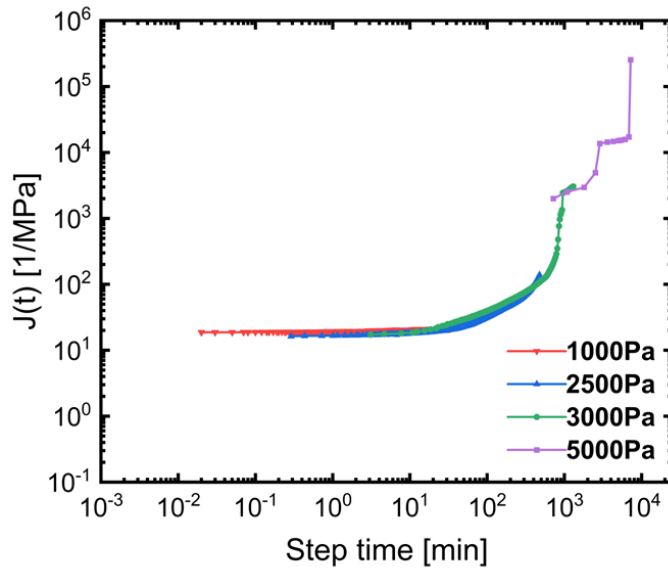


Figure 22. Compliance of the prototype sample at reference stress of 1000 Pa at 110°C.

This strategy can also be employed across different temperatures at a consistent stress level, finding the time required for a known stress to lead to the failure of a product.

Preparations were made and work in underway for conducting tensile creep tests on four different polymers (HDPE, PA, PVDF, Epoxy). The creep tests will involve two types of sample geometries: dog bone samples and double edge notch test (DENT) samples as shown in Figure 23. Figure 24 provides detailed information on the sample geometries. All samples were designed to have a cross-sectional area of 4 mm², ensuring that the applied load can easily reach half the yield stress of the polymer.

The generic material properties obtained from the polymer source are presented in Table 2. Notably, the long-term failure of polyethylene, specifically HDPE, is governed by a slow crack growth (SCG) mechanism [13-14]. SCG describes a brittle mode of polymer failure responsible for reduced service time in industrial applications. HDPE failure due to SCG occurs over extended periods and under low stresses, where low stress is defined as stress below the half yield stress of the material. For the dog bone samples, notches of varying depths (0.5mm to 1mm) will be applied. No additional work is needed to create a notch for the DENT samples, as the notch is incorporated during the design process.

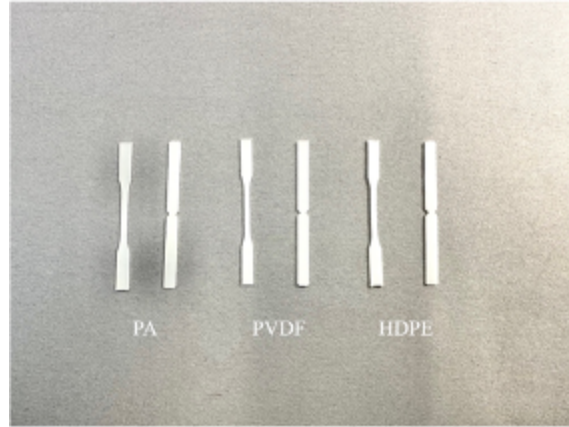


Figure 23. Dog bone and DENT samples of PA, PVDF, HDPE.

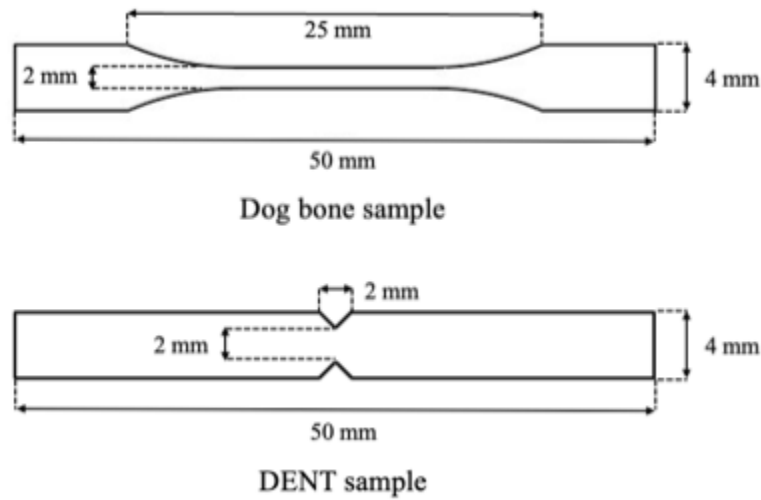


Figure 24. Geometry of dog bone and DENT sample.

Table 2. Material properties from the source of polymers

	Tensile modulus	Flexural modulus
PA	77-84 MPa	2758-3447 MPa
PVDF	42-54 MPa	1792-2137 MPa
HDPE	-	-

As the yield strength and elastic modulus information is not available from the polymer supplier, our approach involves conducting an in-house tensile test to obtain these missing material properties before proceeding with the creep tests. The tensile tests will be performed using the MTS machine depicted in Figure 25. This machine will allow us to characterize the mechanical properties essential for subsequent creep testing such as yield strength and elastic modulus.

Furthermore, Figure 26 illustrates the setup for the creep tests, showcasing a prototype sample. The inclusion of the tensile test ensures a comprehensive understanding of the material's mechanical behavior, enhancing the accuracy and reliability of the subsequent creep tests. This integrated approach provides a more thorough exploration of the polymer's performance under different loading conditions, contributing valuable insights to our research. Early tests show some slipping between the grip and the samples over time and the test design is being modified to ensure no slipping between the tensile loaded samples and the grips in creep tests.

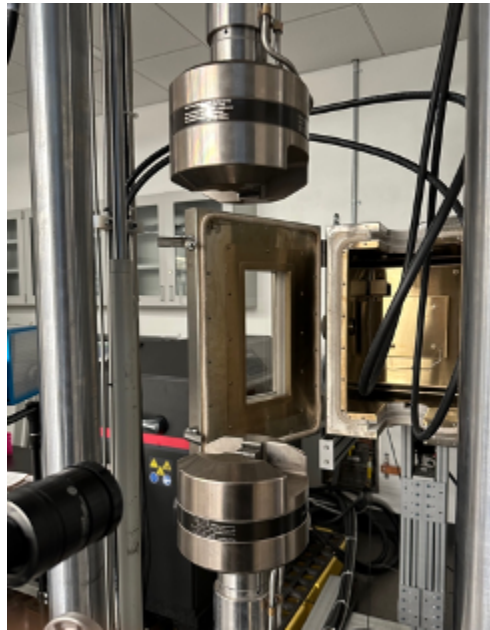


Figure 25. MTS machine for measurement of required material property.

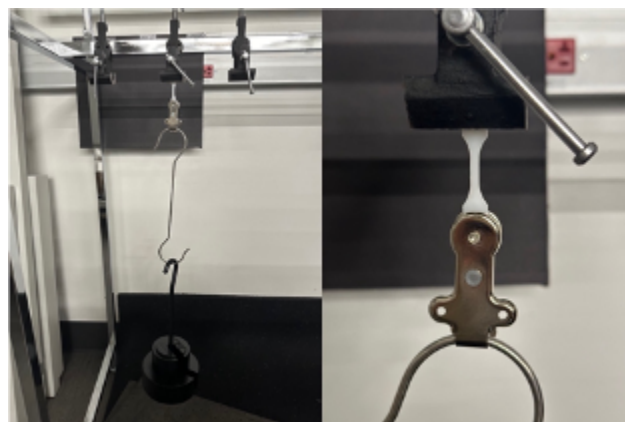


Figure 26. Prototype creep test with current experimental setup.

Project Activities with Cost Share Partners:

Partial support for graduate students is provided as per the cost-share agreement.

References

- [1] Blázquez-Blázquez, E., Pérez, E., Lorenzo, V., & Cerrada, M. L. (2019). Crystalline characteristics and their influence in the Mechanical Performance in Poly (ϵ -caprolactone)/High Density Polyethylene Blends. *Polymers*, *11*(11), 1874.
- [2] Aid, S., Eddhahak, A., Khelladi, S., Ortega, Z., Chaabani, S., & Tcharkhtchi, A. (2019). On the miscibility of PVDF/PMMA polymer blends: Thermodynamics, experimental and numerical investigations. *Polymer Testing*, *73*, 222-231.
- [3] Pawde, S., & Bhat, N. (1994). Thermal analysis of poly (vinylidene fluoride)(PVDF) in composites with polypyrrole (PPY). *Journal of applied polymer science*, *54*(2), 201-205.
- [4] Smith, B. (2021). The infrared spectra of polymers II: polyethylene. *Spectroscopy*, *36*(9), 24-29.
- [5] Li, D., Zhou, L., Wang, X., He, L., & Yang, X. (2019). Effect of crystallinity of polyethylene with different densities on breakdown strength and conductance property. *Materials*, *12*(11), 1746.
- [6] Lambert, S., & Wagner, M. (2018). *Microplastics are contaminants of emerging concern in freshwater environments: an overview* (pp. 1-23). Springer International Publishing.
- [7] Bahrami, M., Abenojar, J., & Martínez, M. A. (2021). Comparative characterization of hot-pressed polyamide 11 and 12: Mechanical, thermal and durability properties. *Polymers*, *13*(20), 3553.
- [8] David, P. S., Karunanithi, A., & Fathima, N. N. (2020). Improved filtration for dye removal using keratin–polyamide blend nanofibrous membranes. *Environmental Science and Pollution Research*, *27*, 45629-45638.
- [9] Ma, N., Liu, W., Ma, L., He, S., Liu, H., Zhang, Z., ... & Zhu, C. (2020). Crystal transition and thermal behavior of Nylon 12. *e-Polymers*, *20*(1), 346-352.
- [10] PIKE Technologies. Analysis of Cured Epoxy Adhesives by ATR / FTIR.
- [11] Mohammadi, M., Yousefi, A. A., & Ehsani, M. (2012). Thermorheological analysis of blend of high- and low-density polyethylenes. *Journal of Polymer Research*, *19*:9798.
- [12] L.S. LEE. (2007). 8 - Creep and time-dependent response of composites, *Woodhead Publishing Series in Civil and Structural Engineering, Durability of Composites for Civil Structural Applications*, Woodhead Publishing, 150-169.
- [13] J. J. Han, et al. (2014) Failure assessment diagram analysis of high density polyethylene pipes, *Journal of Mechanical Science and Technology*.
- [14] H. B. H. Hamouda, et al. (2001) Creep damage mechanisms in polyethylene gas pipes, *Polymer*.